Nanoscale Advances

ROYAL SOCIETY OF CHEMISTRY

PAPER

View Article Online
View Journal | View Issue

Cite this: *Nanoscale Adv.*, 2021, **3**, 3240

A nano-biomimetic transformation system enables *in planta* expression of a reporter gene in mature plants and seeds

Chinenye L. Izuegbunam,[a] Nisitha Wijewantha,[b] Beate Wone,[a] Madhavi A. Ariyarathne,[a] Grigoriy Sereda[b] and Bernard W. M. Wone *[a]

Received 8th February 2021
Accepted 16th April 2021

DOI: 10.1039/d1na00107h

rsc.li/nanoscale-advances

Plant genetic engineering will be essential to decipher the genomic basis of complex traits, optimize crop genomics, and enable plant-based production of recombinant proteins. However, established plant transformation approaches for bioengineering are fraught with limitations. Although nanoparticle-mediated methods show great promise for advancing plant biotechnology, many engineered nanomaterials can have cytotoxic and ecological effects. Here, we demonstrate the efficient uptake of a nano-biomimetic carrier of plasmid DNA and transient expression of a reporter gene in leaves of *Arabidopsis*, common ice plant and tobacco, as well as in the developing seed tissues of *Arabidopsis*, field mustard, barley, and wheat. The nano-biomimetic transformation system described here has all the advantages of other nanoparticle-mediated approaches for passive delivery of genetic cargo into a variety of plant species and is also nontoxic to cells and to the environment for diverse biotechnological applications in plant biology and crop science.

Introduction

Plant genetic engineering will be crucial for deciphering the genetic of basis of complex traits,[1] furthering advances in crop genomics,[2] and enabling plant-based production of recombinant pharmaceutical proteins.[3] Development of a biocompatible transformation system for passive delivery of genetic cargo into a variety of plant species will not only aid in directly testing and deciphering gene function in a variety of plant species but will also facilitate enhanced crop productivity and allow scale-up of the production of recombinant proteins *via* genome manipulation. Increasing crop productivity and environmental stress resistance will be essential to meet the growing food and energy demands of a burgeoning human population under increasingly stressful environmental conditions.[4,5] However, plant genetic engineering depends upon the delivery of genes across the plant cell wall using established methods of genetic transformation that have many disadvantages.[2,6]

Transformation represents a bottleneck for genetic manipulation of plants because of the plant cell wall. Established plant genetic transformation methods rely heavily on *Agrobacterium* to mediate transformation, even though this approach is species-limited. In addition, DNA from *Agrobacterium* remains in the plant host cells, randomly integrates DNA sequences into the plant genome, often resulting in variable transgene expression or insertional mutagenesis.[2,7] Although genome editing is more precise and provides novel opportunities to directly determine gene function or manipulate the genome, it still relies on genetic transformation methods that are also fraught with limitations. Specifically, introducing the CRISPR/Cas9 toolbox into plant cells still depends on *Agrobacterium*-mediated transformation[8] to integrate gene editing components into the plant genome and can still result in undesirable off-target effects[9] and insertional mutations in the genome.[10] Similarly, virus component-mediated transformation of DNA plasmids into plants is species-limited, integrates viral DNA into the host genome, and limits genetic cargo size.[11] Furthermore, this conventional method is subjected to regulatory oversight because of the pathogenic origins of these vectors.[11] Although biolistic DNA plasmid delivery is an efficient method of genetic transformation that does not require *Agrobacterium* or vectors derived from bacteria or viruses, it can result in high frequencies of random plasmid or chromosomal DNA fragment insertion as well as physical injury to the plant.[9,12]

More recently, the use of engineered nanomaterials as gene nanocarriers has shown great promise because nanoparticles can passively enter plant tissues including stems, leaves, roots, and seeds.[13,14] Because of this passive ability to traverse the cell wall and plasma membrane, nanoparticle-mediated delivery of genetic cargo shows great promise for advancing plant genetic engineering.[6] In addition, nanoparticles have high DNA binding ability, high transformation efficiency, and without genome integration.[15–17] Although single-wall carbon nanotubes[15,18]

[a]*Department of Biology, University of South Dakota, SD, USA. E-mail: bernie.wone@usd.edu*

[b]*Department of Chemistry, University of South Dakota, SD, USA*

could be used for such an approach, their major disadvantage for gene introduction is that carbon-based or other highly persistent nanomaterials do not readily break down in organisms or in the environment[19,20] and can disrupt cellular functions.[21] Specifically, carbon nanomaterials including nanotubes, fullerenes, and graphenes are extremely stable and difficult to degrade and thus can be harmful or persist in plant and animal cells or in the environment.[20,22,23] Most importantly, using highly persistent carbon-based nanomaterials to carry DNA plasmids or gene-editing components increases the risk of unwanted and unintended horizontal transfer of heterologous genes to other organisms.[24]

The development of an ideal nanocarrier that is both readily biodegradable and biocompatible has been long awaited in the field of plant transformation. Although biodegradable calcium-based mineral nanoparticles such as calcium phosphate (CaP) have been successfully tested in plants, further explorations of the use of CaP nanoparticles for plant transformation have not yet been further published to our knowledge.[25,26] While CaP nanoparticles describe a general type of particle with various Ca/P ratios and acidities, hydroxyapatite (HA) is the most natural and common form of CaP and is similar to the type of CaP found in mammalian bones and teeth.[27] The use of nano-HAs (nHAs) as novel gene carriers has so far been demonstrated in animal cells,[28–30] bacterial cells,[16,31] and yeast cells,[32] but their effectiveness for gene delivery in plants has yet to be shown. More recently, biocompatible nHAs have been successfully used in biomedical systems to deliver diverse molecular cargo[30,33] and in agricultural systems as synthetic fertilizer.[34,35] Most importantly, synthetic nHAs have many advantages over single-wall carbon nanotubes as gene carriers for plants[15,18] because they are noncytotoxic[22,33,34] and nonecotoxic,[36,37] readily broken down and used by plants as nutrients,[38,39] and can be harmlessly assimilated by either plant or animal cells or the environment.[33] Therefore, nHAs can be considered as nano-biomimetic gene carriers.[40–42]

Here, we report the use of biocompatible and optimizable nHA-based DNA carriers to passively deliver DNA plasmids for genetic transformation *in planta* to further advance the nanoparticle-mediated transformation approach. We have synthesized and validated a system for highly efficient, passive, and harmless genetic transformation of both model and crop plants. We have used nHAs functionalized with arginine for transient *in vivo* infiltration of plasmid–nHA conjugates into leaves of tobacco (*Nicotiana benthamiana*), *Arabidopsis*, and common ice plant (*Mesembryanthemum crystallinum*) and have observed protein expression from introduced transgenes. We have also shown strong protein expression in germinating seeds of *Arabidopsis*, field mustard (*Brassica rapa*), wheat (*Triticum aestivum*), and barley (*Hordeum vulgare* L.) after incubation in a solution of plasmid–nHA conjugates. The present study demonstrates highly efficient, passive, and harmless delivery of genetic cargo with less potential for horizontal transfer of recombinant genes by the nanocarrier. This combination of highly desirable features is not achievable with either current nanoparticle-mediated or established transformation approaches. Altogether, the nano-biomimetic transformation system will revolutionize plant genetic engineering, the ability to investigate the genomic basis of traits, and the ability to manipulate the genomes of a wide variety of plants for many possible biotechnology applications.

Materials and methods

Synthesis of nanohydroxyapatites

Rod-shaped nanohydroxyapatites (nHAs) 10 nm in diameter were synthesized following the procedure of Huang *et al.*[43] To minimize particle aggregation, the nHAs were prepared in the presence of the nontoxic, nonionic biocompatible surfactant PEG 300 as a chemical dispersant.[44] An aliquot of PEG-300 (1336 ml) was added by micropipette to a 100 ml volumetric flask and the volume was brought to 100 ml with deionized water to prepare a 1.5% (w/w) aqueous solution of PEG. The prepared PEG solution was mixed with 0.5549 g of $CaCl_2$ to prepare 100 ml of $CaCl_2$ solution (0.05 M, 100 ml). The resulting solution was equilibrated overnight (about 12 h) at room temperature (RT) and then added dropwise (1.6 ml min^{-1}) into 100 ml of 0.03 M aqueous Na_2HPO_4 solution with mechanical stirring at a constant speed of 1000 rpm. The resulting solution was placed in a closed glass vial and incubated for 48 h at RT. After 48 h, the solution was centrifuged at 11 000 rpm for 10 min to separate the white precipitate. The separated white precipitate was washed three times with deionized water (Thermo Scientific™, Barnstead™ Nanopure), and then three times with absolute ethanol, and finally dried at 60 °C overnight to obtain the as-prepared powder product, which was then calcined at 500 °C for 2 h to produce the nHAs.

Arginine-functionalized nanohydroxyapatites

Nanohydroxyapatites (100 mg) were functionalized following the procedure of Deshmukh *et al.*[16] with a slight modification. Briefly, nHAs were functionalized by mixing them with a solution of positively charged arginine (100 ml, 0.1 wt%). The mixture was stirred at 600 rpm for 1 h. The functionalized particles were separated and washed three times with deionized water followed by centrifugation at 8000 rpm for 10 min. The washed particles were dried at ambient temperature overnight (about 12 h) to obtain about 310 mg of arginine-functionalized nHAs (R-nHAs).

Characterization of nanohydroxyapatites

Scanning electron microscopy. A 5 mg sample of the synthesized nHAs was dispersed in ethanol (10 ml) using an ultrasonication probe. One droplet of the dispersion was deposited onto the reflective face of a silicon wafer and dried at 600 °C for 30 min for SEM imaging. Particle sizes and shapes were imaged using a Zeiss Sigma Field Emission Scanning Electron Microscope (SEM) with an accelerating voltage of 4 kV (Carl Zeiss Microscopy, LLC, White Plains, NY, USA).

Transmission electron microscopy. Synthesized nHAs (1 mg) or R-nHAs (1 mg) were dispersed in 20 ml of deionized water and one droplet of each suspension was deposited onto copper-coated TEM grids for imaging and air-dried for 2 d in a vacuum

desiccator. Nanoparticle morphologies were imaged using a FEI Tecnai G2 TWIN TEM with an accelerating voltage of 120 kV (Field Electron and Ion Company, Hillsboro, OR, USA).

Powder X-ray diffraction. High-angle powder X-ray diffraction (PXRD) patterns for nHAs and R-nHAs were recorded on a Rigaku Ultima IV XRD Diffractometer (Rigaku Analytical Devices, Inc., Wilmington, MA, USA) using Cu Kα radiation (λ = 1.54 Å, 40 kV, 44 mA). The diffraction spectra were collected over a range of 15° to 80° with a 0.02° sampling width.

Zeta potential measurement. The surface zeta potential measurements of nHAs and R-nHAs (before and after arginine functionalization) were performed on a Malvern Zetasizer ZS Nano S Instrument (Malvern Panalytical Ltd., Malvern, UK).

Energy dispersive spectroscopy analysis. For the energy dispersive spectroscopy (EDS) analysis, a small amount of nHA powder was placed on self-adhesive carbon tape and sputter-coated with 28 nm of carbon using a Denton Desk V TSC sputter coating accessory (Denton, Moorestown, NJ, USA). An Oxford Instruments X-Max^N 50 EDS probe (Oxford Instruments NanoAnalysis, Concord, MA, USA) was used to conduct elemental analysis of prepared nHAs with the probe attached to a ZEISS Sigma Field Emission SEM.

Plant growth

Arabidopsis thaliana, ice plant, and tobacco plants were grown in Miracle-Gro® Moisture Control® Potting Mix (The Scotts Company LLC, Marysville, OH, USA) under a 16 h day : 8 h night photoperiod at ~22 °C in an environmentally controlled room. Barley seeds and wheat seeds were obtained from http://www.Amazon.com, and field mustard seeds were obtained from http://www.toddsseeds.com.

Cloning and plasmid isolation of pGWB402::GUS

The gene encoding β-glucuronidase (GUS) with flanking attL and attR sites was synthesized by Gene Universal (Newark, DE, USA). The pGWB402::GUS construct was generated using the LR cloning reaction with pGWB402 expression vector and the synthesized GUS-encoding gene. The resulting plasmid pGWB402::GUS was transformed into 10-beta competent *Escherichia coli* cells (New England Biolabs, Ipswich, MA, USA). Plasmid DNA was extracted from the *E. coli* cells using the Qiagen Plasmid Mini Kit (Qiagen, Hilden, Germany). The 11 833 bp pGWB402::GUS vector is referred to as pDNA herein.

Preparation of pDNA–nHA and pDNA–R-nHA conjugate

R-nHA and the pDNA carrying the reporter gene encoding β-glucuronidase (GUS) was used to prepare pDNA–R-nHA conjugates following the procedure of del Valle *et al.*[31] with modifications. Briefly, an aqueous suspension of 1 mg ml^{-1} of R-nHA was evenly dispersed by sonicating in an ice bath for 10 min. One μg of pDNA and 200 μg of R-nHA was used to make a 1 : 200 pDNA : R-nHA w : w ratio conjugate mixture. The 1 : 200 pDNA : R-nHA ratio conjugate mixture was then thoroughly mixed by vortexing for 30 s. After vortexing, the mixture was incubated at 37 °C with shaking at 200 rpm for 90 min. Unbound pDNA was removed by centrifugation at 10 000 rpm for 10 min. The precipitate was resuspended in 10 ml of 0.5% low-viscosity carboxymethylcellulose (CMC) and stirred for 2 h at RT to keep the pDNA–R-nHA conjugates in suspension.[45] The formation of pDNA–R-nHA conjugates was visualized on 1% agarose gel.

pDNA conjugating efficiency

The efficiency of pDNA conjugating to R-nHA was assessed following the procedure of Deshmukh *et al.*[32] Briefly, aqueous 1 mg ml^{-1} suspensions of R-nHA were prepared by sonicating for 10 min on ice. An aliquot 500 ng of pDNA was mixed with R-nHA suspensions at different w : w ratios (1 : 10, 1 : 30, 1 : 50, 1 : 70, 1 : 100, 1 : 200). The mixtures were shaken at 37 °C for 10 min at 200 rpm and centrifuged at 15 000 rpm for 4 min. The supernatant containing the unbound pDNA was used to determine the conjugating efficiency of R-nHA to pDNA. The optical density of the supernatant was determined at 260 nm relative to the supernatants from R-nHA without pDNA as blanks. The DNA conjugating efficiencies (CEs) were determined using the equation:

$$\%\ \mathrm{CE} = \{[(\mathrm{pDNA})\mathrm{i} - (\mathrm{pDNA})\mathrm{f}]/[(\mathrm{pDNA})\mathrm{i}]\} \times 100,$$

where % CE = percent conjugating efficiency, [pDNA]i = the optical density of the initial amount of pDNA added to the reaction mixture, and [pDNA]f = the optical density of the unbound pDNA remaining in the sample. The assay was independently repeated three times with three technical replicates per assay. The pellets were dissolved in 50 μl of DNase/RNase free water and 10 μl of the pDNA–R-nHA conjugates were separated on 1% agarose gel to confirm conjugation of pDNA to R-nHA.

Nuclease digestion

The 1 : 200 ratio (w : w) pDNA–R-nHA conjugates were prepared as described above, and 100 ng aliquots of the precipitates were resuspended in 20 μl of Dnase/RNase free water, respectively. DNase 1 (250 U μl^{-1}) (Zymo Research, Tustin, CA, USA) was added (1 μl) to the resuspended pDNA–R-nHA conjugates and digestion allowed to proceed for 1 h at RT. After incubation, samples were mixed with 2 μl of 6× loading dye (New England Biolabs Ltd., Ipswich, MA, USA) and loaded onto 1% w/v agarose for electrophoresis. Samples of digested and undigested pDNA or undigested pDNA–R-nHA were used as controls.

Transient expression

***Agrobacterium*-mediated transformation.** *Agrobacterium*-mediated transformation was used as a positive control for *in vivo* transient expression infiltrations using the pDNA–R-nHA conjugates. The vector pGWB402::GUS was transformed into *Agrobacterium* strain GV3101 using the freeze–thaw method of Wise *et al.*[46] A single *Agrobacterium* colony was inoculated into liquid Luria–Bertani (LB) medium containing the appropriate antibiotics for binary vector selection. This feeder culture was incubated at 28 °C, 250 rpm for 2 d. Then the feeder culture was centrifuged at 3000 rpm for 10 min at RT and the supernatant

discarded. The pellet was resuspended in infiltration buffer (10 mM MES, 10 mM $MgCl_2$, pH = 5.6). Centrifugation and resuspension steps were repeated three times to remove any remaining LB to stop *Agrobacterium* growth. The bacterial pellet was resuspended in the infiltration buffer to obtain a 1 : 10 dilution ($OD_{600} \sim 0.5$) and acetosyringone was added to the infiltrate to a final concentration of 200 μM. Tobacco leaves were infiltrated using the syringe infiltration method of Leuzinger *et al.*[47] and incubated for 3 d in an environmentally controlled room before performing GUS assays.

***In planta* pDNA–R-nHA leaf infiltration.** A 1 : 200 (w : w) pDNA–R-nHA conjugate was used for plant leaf infiltration. Briefly, the pDNA–R-nHA mixture was shaken for 90 min at 200 rpm at 37 °C. Unbound pDNA was removed by centrifugation

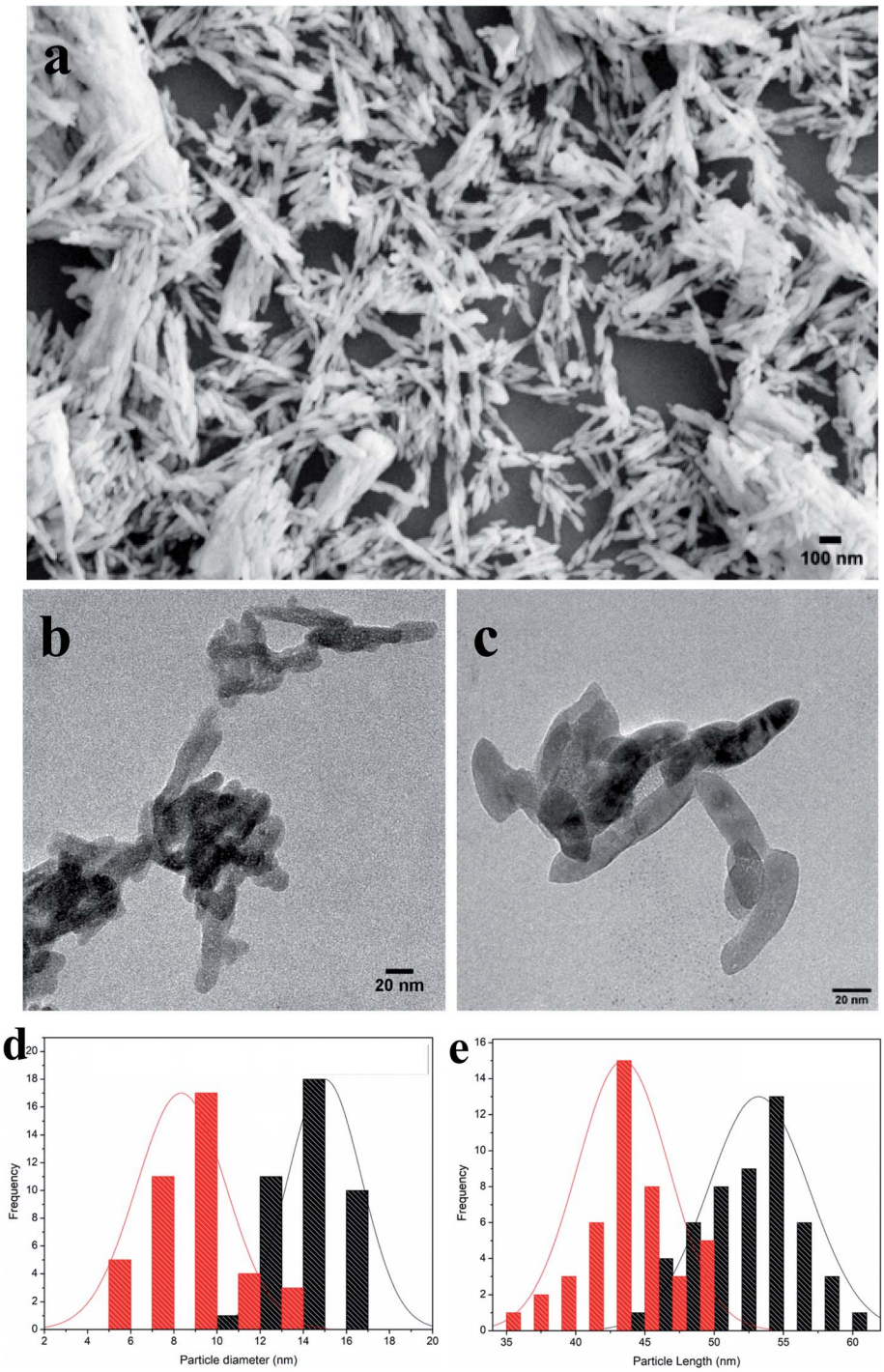

Fig. 1 Morphologies of synthesized nanohydroxyapatites (nHAs). (a) Scanning Electron Microscope (SEM) image of nHAs. (b) Transmission Electron Microscope (TEM) image of nHAs. (c) TEM image of arginine-functionalized nHAs (R-nHA). Scale bars: 100 nm (a); and 20 nm (b and c). (d) Distribution of particle diameters (nm) in nHAs (red colored columns) and R-nHAs (black colored columns). (e) Distribution of particle lengths (nm) in nHAs (red colored columns) and R-nHAs (black colored columns).

at 10 000 rpm for 10 min. The precipitate was resuspended in 10 ml of aqueous 0.5% low-viscosity CMC and stirred for 2 h at room temperature to keep the R-nHA particles suspended.[45] The formation of pDNA–R-nHA conjugates was visualized on 1% agarose gel. Mature *Arabidopsis* and tobacco leaves were infiltrated using a syringe and left for 3 d in an environmentally controlled room prior to performing GUS assays.

Healthy leaves of *Arabidopsis*, tobacco, and ice plant were detached from whole plants and transferred into Petri dishes containing pDNA–R-nHA suspended in 0.5% CMC. The solution was vacuum infiltrated into the leaves at −0.01 MPa for 1 min following the procedure of Leuzinger *et al.*[47] and the process was repeated twice before transferring the dishes containing the infiltrated leaves to an environmentally controlled room. The leaves were kept moist in water for 4 d prior to assaying for GUS expression. The experiment was repeated three times.

Incubation of seeds in a solution of pDNA–R-nHA conjugates. Seeds of common wheat, field mustard, and barley were pre-soaked in water (*i.e.*, control), or in a solution of pDNA–R-nHA conjugates for 15 min and then vacuum infiltrated at −0.01 mPA for 1 min. Vacuum infiltration was repeated three times at 15 min intervals. The common wheat, and barley seeds were kept moist for 4 d before testing for expression of the gene encoding GUS, whereas field mustard seeds were kept moist for 6 d to allow the seeds to sprout before testing for expression of

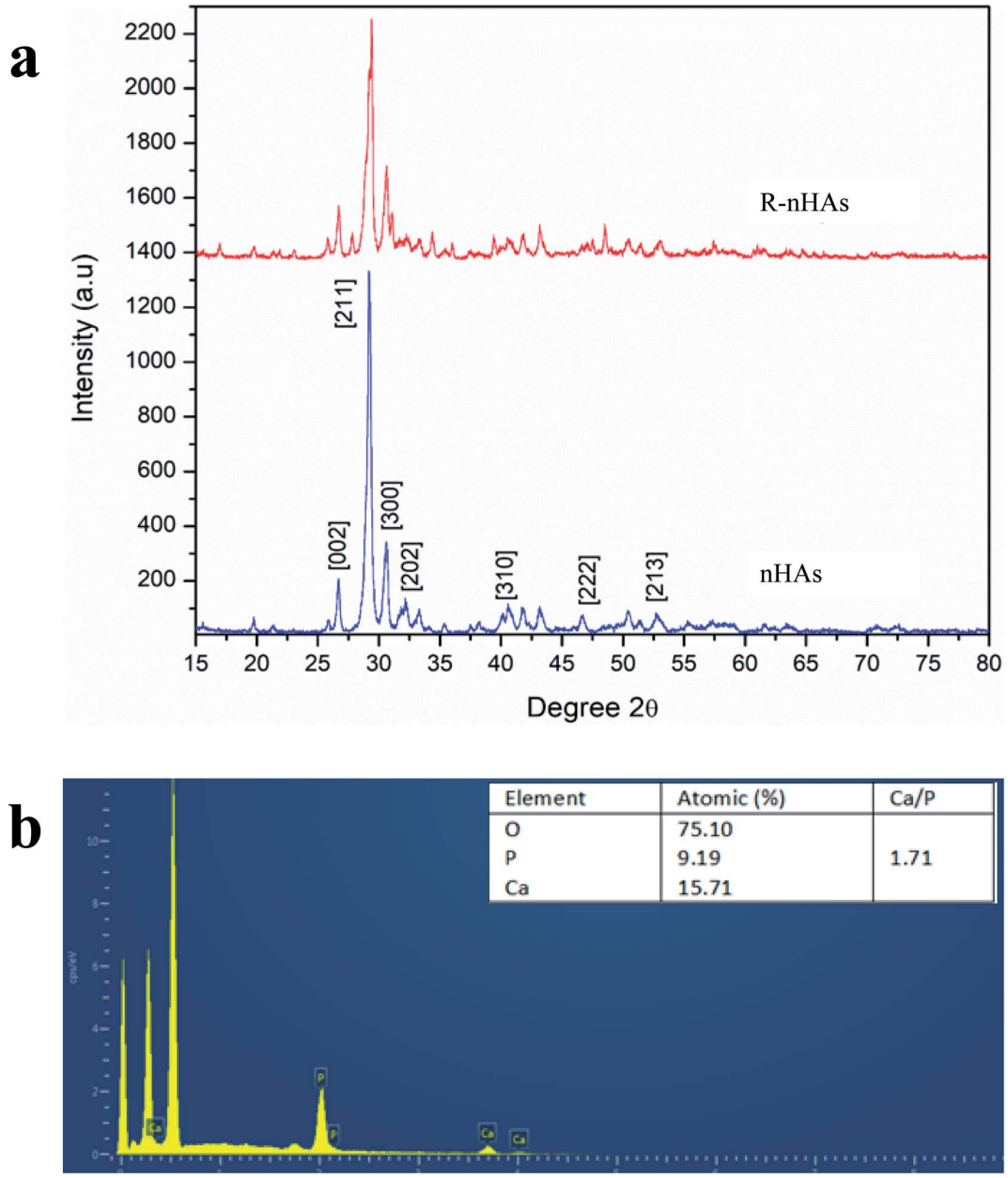

Fig. 2 Physicochemical characteristics of nanohydroxyapatites (nHAs). (a) Powdered X-ray diffraction (PXRD) pattern of nHAs and R-nHAs (functionalized with arginine). (b) Energy Dispersive Spectroscopy (EDS) spectra of nHAs, where measured Ca/P ratio is ~1.71.

the gene encoding GUS. Germinated seeds of *Arabidopsis* and field mustard were also pre-soaked in water (*i.e.*, control), or in a solution of pDNA–R-nHA conjugates, where the pDNA was a vector carrying a G3 green fluorescent protein gene (*i.e.*, G3GFP in pGWB542). GFP fluorescence was visualized after 3 d using a Leica DMRA2 fluorescence microscope with a Leica DFC3000 G camera (Leica Microsystems Inc., Buffalo Grove, IL).

GUS assay. The GUS assay solution was prepared following the procedure of Lim *et al.*[48] by dissolving 0.5 mg ml^{-1} of X-Gluc (5-bromo-4-chloro-3-indolyl glucuronide) in GUS assay buffer (50 mM sodium phosphate buffer, pH 7.0; 0.1 mM $K_4Fe(CN)_6$; 0.1 mM $K_3Fe(CN)_6$; and 4 mM EDTA). The GUS assay solution was introduced into the seeds by vacuum infiltration at −0.07 MPa for 10 min. The infiltrated seeds were incubated for 36 h at 37 °C and chlorophyll removed in 100% ethanol overnight before images were captured using a Leica EZ24 HD Stereo Microscope (Leica Microsystems Inc., Buffalo Grove, IL).

Results and discussion

Characterization of arginine-functionalized nHA nanoparticles

Nanohydroxyapatite rods were synthesized to carry genetic cargo for passive uptake and *in planta* transformation. Because

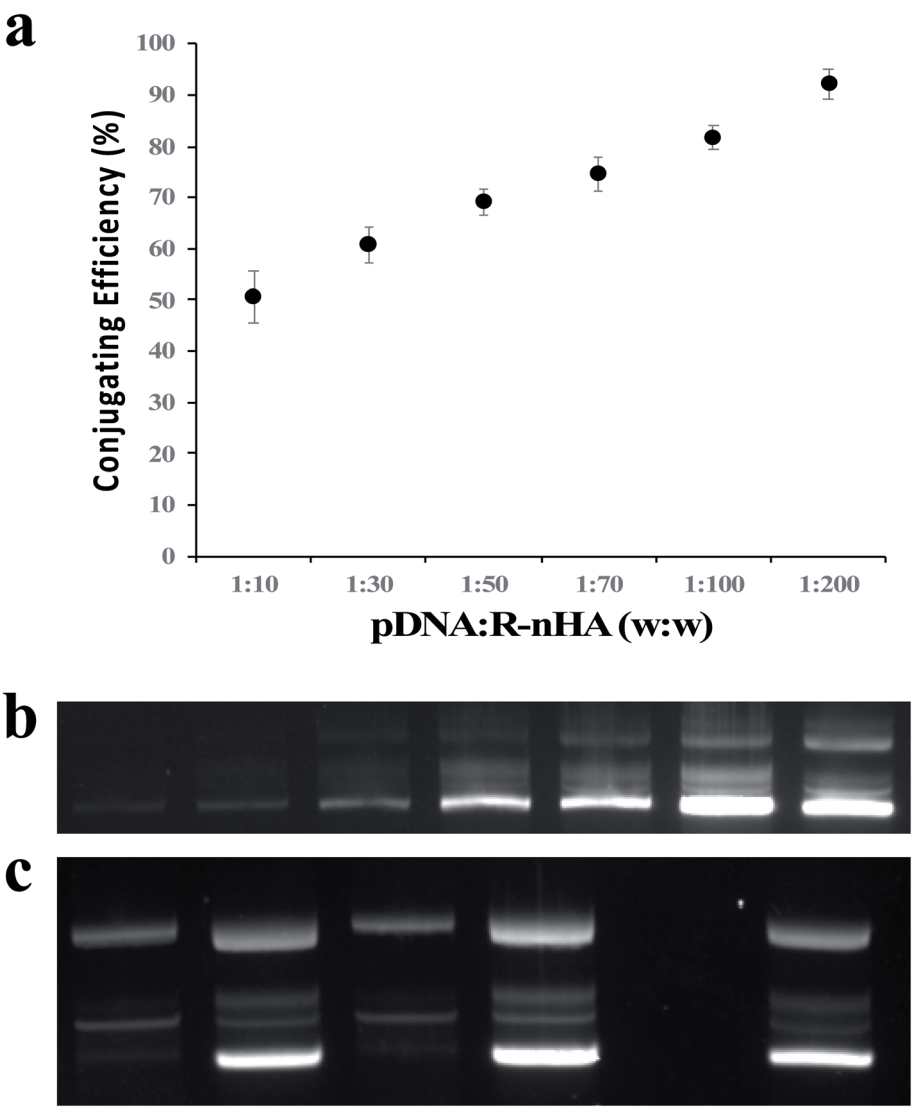

Fig. 3 Conjugation of DNA plasmid (pDNA) with nanohydroxyapatites (nHAs). (a) Conjugation efficiency assay of pDNA and R-nHAs by measuring the optical density of the supernatant (*i.e.*, unbound pDNA in an aqueous solution of water) at 260 nm indicates the 1 : 200 mass ratio conjugates have the highest conjugating efficiencies. Error bars are standard error of the mean ($n = 3$). (b) Agarose gel electrophoretogram of pDNA–R-nHA conjugates confirms the 1 : 200 mass ratio conjugates is the most efficient ratio as indicated by the bright intensity of the band in lane 6. Lane 1 – 1 : 10 mass ratio. Lane 2 – 1 : 30 mass ratio. Lane 3 – 1 : 50 mass ratio. Lane 4 – 1 : 70 mass ratio. Lane 5 – 1 : 100 mass ratio. Lane 6 – 1 : 200 mass ratio. Lane 7 – pDNA. Faint bands indicate relaxed and supercoiled (bright bands) conformations of pDNA or pDNA–R-nHA conjugates. (c) DNase assay of conjugates suggests nHAs might reduce or inhibit endonuclease activity, especially relaxed forms of the plasmid. Lane 1 – pDNA–R-nHA conjugates with DNase treatment. Lane 2 – pDNA–R-nHA conjugates without DNase treatment. Lane 3 – pDNA–nHA conjugates with DNase treatment. Lane 4 – pDNA–nHA conjugates without DNase treatment. Lane 5 – pDNA with DNase treatment. Lane 6 – pDNA without DNase treatment. Faint bands indicate relaxed and supercoiled (bright bands) conformations of pDNA or pDNA–nHA conjugates.

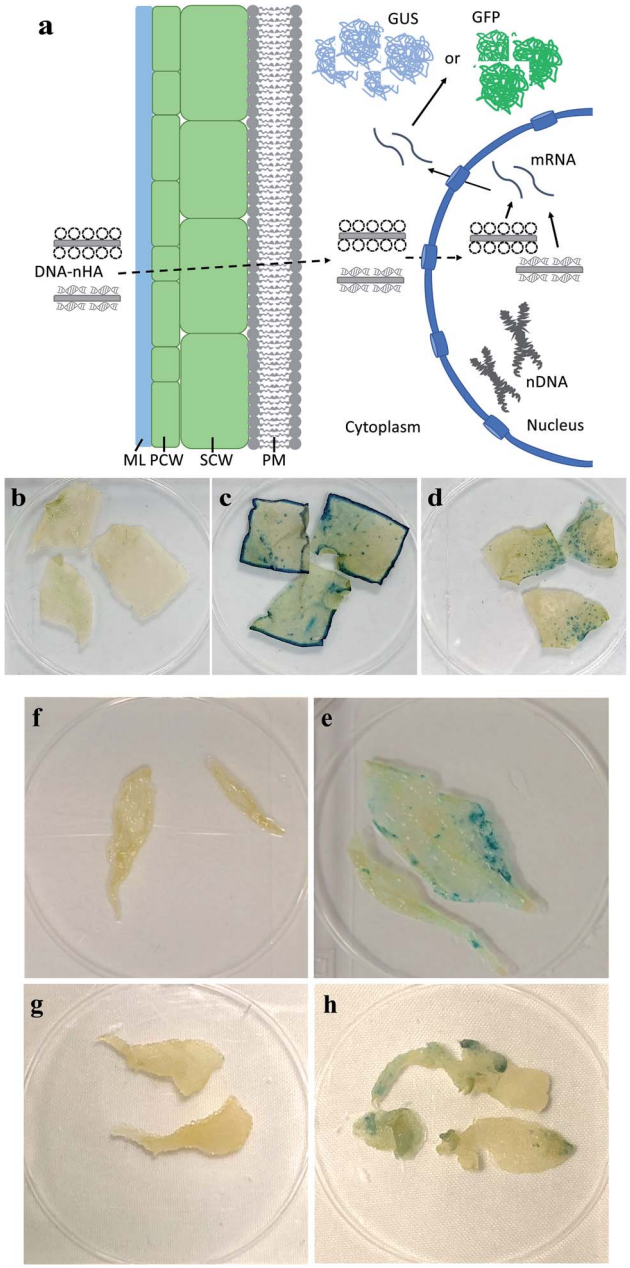

Fig. 4 Plasmid DNA (pDNA) delivery into mature leaves with arginine-functionalized nanohydroxyapatites (R-nHAs) and subsequent GUS expression. (a) Model of uptake and translocation of DNA–nHA conjugates and subsequent expression of introduced gene(s) in a plant cell. Dotted-line arrows represent trafficking of complexes, whereas solid-line arrows represent expression of introduced gene(s). DNA–nHA – plasmids or PCR amplicons conjugated to nHA. ML – middle lamella. PCW – primary cell wall. SCW – secondary cell wall. PM – plasma membrane. nDNA – nuclear DNA. mRNA – messenger RNA. GUS – stained GUS protein product. GFP – GFP product. (b–h) Transient GUS expression in leaves of mature tobacco (*Nicotiana benthamiana*) and *Arabidopsis thaliana* after *in vivo* infiltration of pDNA–R-nHA conjugates of healthy plants using a syringe, and *Arabidopsis*, and ice plant (*Mesembryanthemum crystallinum*) after vacuum infiltration of pDNA–R-nHA conjugates in detached leaves from healthy plants: (b) control (untreated) – tobacco; (c) *Agrobacterium*-mediated expression of GUS in tobacco; (d) pDNA–R-nHA-mediated expression of GUS in tobacco; (e) control (untreated – infiltrated with water) – *Arabidopsis*; (f) pDNA–R-nHA-mediated expression of GUS in *Arabidopsis*; (g) control (untreated – infiltrated with water) – ice plant; and (h) pDNA–R-nHA-mediated expression of GUS in ice plant. Blue spots or patches (arrows) represent histochemical staining of GUS.

the size exclusion limit of plant cell walls is ~5–20 nm,[13,14] we synthesized ~10 nm diameter nHAs following the method of Huang *et al.*[43] The sizes and morphologies of these nHAs were confirmed by SEM and TEM. SEM and TEM imaging confirmed that we achieved thin-rod morphologies with an average diameter of 8.5 nm and an average length of 42 nm (Fig. 1a–c). These nHAs were then functionalized with arginine (R) to enhance the electrostatic interactions between the nanoparticles and plasmid DNA (pDNA) for improved pDNA–nHA conjugate formation. The nanohydroxyapatite particles functionalized with arginine (R-nHAs) exhibited slight changes in average diameters from 8.5 nm to 15 nm and average lengths of from 42 nm to 55 nm, respectively (Fig. 1c). The surface zeta potential measurements changed slightly from -19.9 mV $\pm$ 2.3 mV for nHAs to -12.8 mV $\pm$ 1.6 mV for nHAs functionalized with arginine. This increase was attributed to the introduction of the positively charged arginine amino and guanidinium groups to the particle surfaces. Furthermore, the powder X-ray diffraction (PXRD) patterns of the synthesized nHAs showed diffraction characteristic of nHA nanorods (Fig. 2a). PXRD spectra illustrated that both the nHAs and R-nHAs have diffraction peaks at 2θ values of 26.2, 29.9, 31.2, 34.1, 40, 46.4, and 53, which are attributable to the (002), (211), (300), (202), (310), (222), and (213) diffraction planes of the hydroxyapatite phase, respectively. These diffraction peaks confirmed the formation of hydroxyapatite nanocrystals. The patterns of the PXRD peaks for the R-nHAs remained unchanged after functionalization. The surface calcium/phosphate ratio of 1.71 for the synthesized nHAs determined by Energy Dispersive Spectroscopy (EDS) was found to be 1.71, which is close to the theoretical value of 1.66 for hydroxyapatite (Fig. 2b).

Conjugation of plasmid DNA to R-nHA

To determine the ability of pDNA to conjugate with R-nHA, we investigated the conjugating efficiency (CE) of test pDNAs to R-nHA by generating pDNA–nanoparticle conjugates with various mass ratios (w : w) ranging from 1 : 10 to 1 : 200. The conjugates were centrifuged to collect the supernatant containing the unbound pDNA. The amount of the unbound pDNA in the supernatant was then determined by measuring the optical density of the supernatant at 260 nm. CE was highest for the conjugates with 1 : 100 and 1 : 200 mass ratios (Fig. 3a). Conjugate formation was further confirmed by subjecting the recovered pellets from different ratios to gel agarose electrophoresis (Fig. 3b). To assess the stability of the pDNA–nanoparticle conjugates, we treated the 1 : 200 ratio pDNA conjugates to R-nHA with DNase 1 endonuclease. The test pDNAs conjugated well to R-nHA and the relaxed forms of the pDNA in particular were also partly protected from the DNAse 1 endonuclease, suggesting that nHAs might reduce or inhibit endonuclease activity (Fig. 3c).

R-nHA-mediated delivery of DNA plasmid into mature leaves

To demonstrate *in vivo* delivery of pDNA and transient expression in leaves using R-nHA carriers, mature leaves of *Arabidopsis*, tobacco, and common ice plant were infiltrated with a solution of pDNA–R-nHA conjugates. We tested the efficacy of transformation with pDNA–R-nHA conjugates in these plant species in order to demonstrate the utility of our system for delivering plasmids into a wide variety of model, and other plant species. Solutions of pDNA–R-nHA conjugates carrying a GUS-encoding reporter gene were injected into intact mature leaves using a syringe or infiltrated into detached leaves in a dish under vacuum. We hypothesized that the pDNA–R-nHA conjugates introduced into leaves would traverse the cell wall and travel into the nucleus where the GUS reporter gene carried on the pDNA would be expressed (Fig. 4a). After 2–3 d, leaves were assayed by histochemical staining for GUS followed by clearing of chlorophyll using ethanol. Transient GUS expression was observed in the leaves as characteristic blue spots or patches within leaf tissues (Fig. 4d–h).

R-nHA-mediated transformation of seeds

We incubated seeds of field mustard, wheat, and barley in solutions of pDNA–R-nHA conjugates and then compared transient reporter gene expression in seeds of eudicot field mustard to those of monocot wheat and barley to ensure that the pDNA–R-nHA conjugates could transform germinating seeds and to demonstrate the applicability of our system for genetic transformation of seeds of crop species from both of these paraphyletic groups. At 4 d after a 1 h incubation in a solution of pDNA–R-nHA conjugates, GUS protein expression was confirmed by examining seeds under a dissecting microscope after histochemical staining for GUS activity. GUS protein

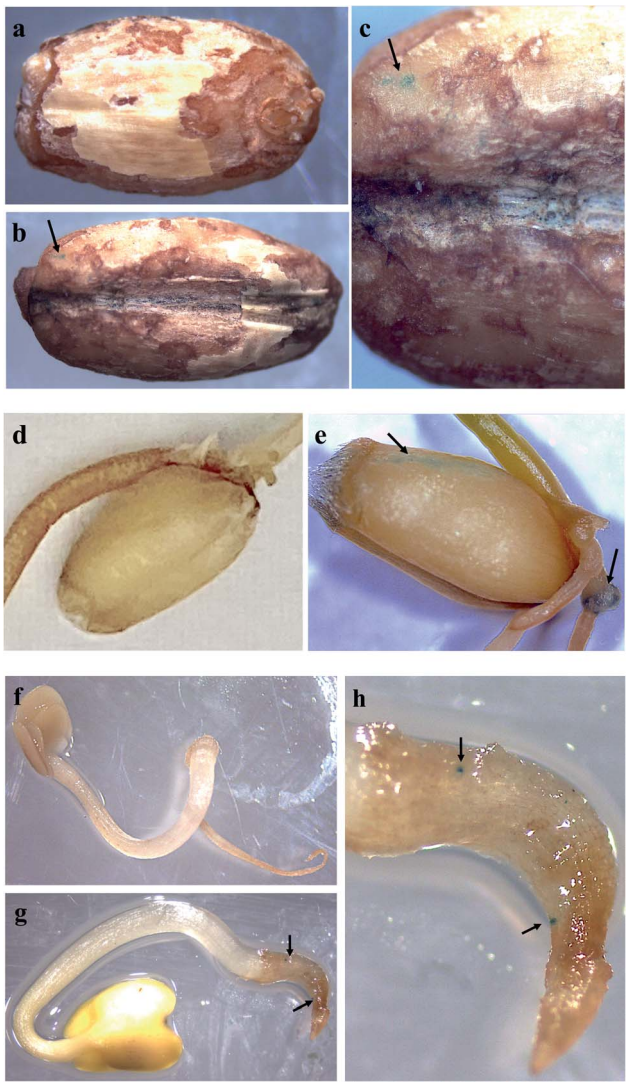

Fig. 5 Plasmid DNA (pDNA) delivery into seeds with arginine-functionalized nanohydroxyapatites (R-nHAs) *via* incubation in a solution of pDNA–R-nHA conjugates and subsequent GUS expression. (a) Control (untreated – incubated in water) – barley (*Hordeum vulgare*) seed. (b) Transient GUS expression in imbibed barley seed after incubation in a solution of pDNA–R-nHA conjugates. (c) Magnification at 25× of the barley seedling. (d) Control (untreated – incubated in water) – wheat (*Triticum aestivum*) seed. (e) Transient GUS expression in imbibed wheat seed after incubation in a solution of pDNA–R-nHA conjugates. Arrow indicates embryonic tissue expressing GUS. (f) Control (untreated – incubated in water) – *Brassica rapa* seed at 8× magnification. (g) Transient GUS expression in imbibed *Brassica rapa* seed after incubation in a solution of pDNA–R-nHA conjugates. Magnification at 8× of developing seedling. (h) Magnification at 15× of the seedling radical. Blue spots or patches (arrows) represent histochemical staining of GUS in all the panels.

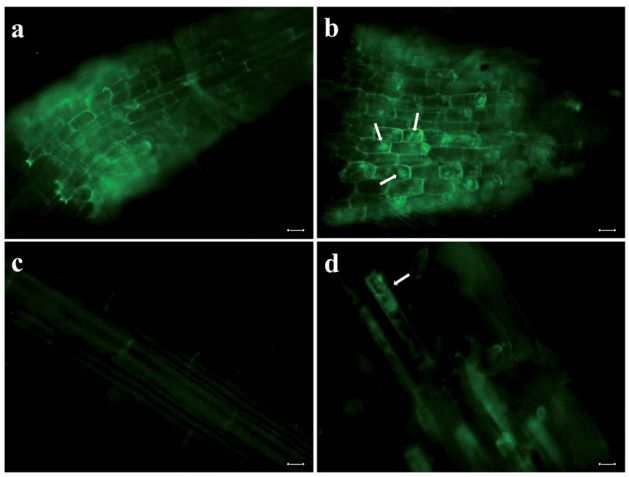

Fig. 6 Delivery of plasmid DNA (pDNA) with green fluorescent protein gene into root cells of seedlings with arginine-functionalized nanohydroxyapatites (R-nHAs) *via* incubation in a solution of pDNA–R-nHA conjugates and subsequent GFP expression. (a) Root cells of 4 d old *Arabidopsis* seedling after incubation in water (*i.e.*, control). (b) Transient GFP expression in imbibed root cells of 4 d *Arabidopsis* seedling after incubation in a solution of pDNA–R-nHA conjugates. (c) Root cells of 4 d field mustard (*Brassica rapa*) seedling after incubation in water (*i.e.*, control). (d) Transient GFP expression in imbibed root cells of 4 d field mustard seedling after incubation in a solution of pDNA–R-nHA conjugates. Green patches (arrows) indicate GFP protein expression in cytoplasm of root cells in panels b and d, whereas the green outline of the cell is due to autofluorescence of lignin in the cell wall in all panels. All images are at 100× magnification. Scale bars: 20 μm.

was expressed in all seeds subjected to the transformation protocol, and most interestingly in the developing embryonic tissues of wheat, and field mustard (Fig. 5a and h). In addition, GFP protein expression was observed in the cytoplasm as green patches within root cells as predicted (Fig. 4a) in both *Arabidopsis* and field mustard seedlings (Fig. 6a–d).

GUS expression was not observed in the developing embryonic tissue of barley, as it takes more than six days to germinate and thus transient GUS expression would not be observable when germination finally occurs. The expression of GUS activity in developing embryonic tissues of wheat, barley and field mustard suggest that our system for delivery of genetic cargo has very high potential for stable genetic transformation of germline tissues in seeds or even in reproductive organs. Altogether, our R-nHA-based plasmid DNA delivery method enables passive delivery of DNA into both leaf cells and germinating seeds of several plant species with high efficiency and no observable adverse effects on germination.

Conclusions

We have demonstrated *in planta* genetic transformation of tissues in mature plant leaves and germinating seeds using a nano-biomimetic carrier for genetic cargo. Our system uses synthesized R-nHAs as nanocarriers to allow pDNA to traverse plant cell walls and be delivered into leaf or root cells. By using a pDNA carrying a GUS or GFP reporter gene, we have shown successful delivery and transient heterologous gene expression in germinating seeds of *Arabidopsis*, wheat, barley, field mustard, as well as in detached and intact mature leaves of *Arabidopsis*, tobacco, and common ice plant. This passive transformation system has all the advantages of other nanoparticle-mediated approaches including that it is simple, rapid, cost-effective, nondestructive, species-independent, scalable, and optimizable, and also eliminates unwanted integration of vector sequences into the target genome.[15,18] These nanocarriers also possess the further advantages of noncytotoxicity, ready biodegradability, biocompatibility, and less potential for horizontal transfer of genetic cargo.

Nanoparticle-mediated gene delivery has immense promise for advancing plant genetic engineering because nanoparticles are cell wall-permeable; however, their use has raised some concerns regarding the health of organisms and ecosystems.[21,49] Notably, some engineered nanomaterials, especially carbon-based forms, are difficult to break down or can be cytotoxic to both animals and plants. Their harmful effects can include generation of reactive oxygen species, DNA damage, lysosomal damage, mitochondrial dysfunction, and eventual cell death *via* apoptosis or necrosis.[23,49–51] Some engineered nanomaterials can also activate various immune cells or induce immunosuppression.[23] Although the physicochemical properties of highly persistent engineered nanomaterials can be functionalized so that they are then less cytotoxic or noncytotoxic, their extreme stability and resistance to degradation might result in their bioaccumulation in organisms and the environment.[52,53] Undeniably, one of the critical issues regarding engineered nanomaterials as gene carriers for plants is the potential for horizontal transfer of recombinant genes conjugated to the engineered nanomaterials to nontarget organisms, especially if the carrier does not readily break down. Specifically, recombinant genes conjugated to nanomaterials can be directly or indirectly transferred to nontarget plant species including weedy species.[24,54–56] In contrast, because nHA-based nanomaterials are readily broken down within plants[38,39] and conjugated recombinant genes can then be digested by endogenous nucleases, horizontal transfer of recombinant genes to nontarget organisms will be much less likely. In addition, because nHAs are composed of the elements Ca and P, their broken-down components could provide an excellent form of nutrients for plants.[34,35,38] For instance, application of nHAs or HAs as a fertilizer enhanced the germination and radicle growth of chickpea (*Cicer arietinum*) seeds,[38] increased the growth rate and yield of soybean plants,[45] and increased the growth of lettuce (*Lactuca sativa* L.) plants[35] without adverse impacts on the growth of soil bacteria.[34] Interestingly, nHAs can also reduce the mobility of lead in the rhizosphere and toxicity of lead in roots of rice.[57] Altogether, the above characteristics of nHAs make them ideal components of a nano-biomimetic plant transformation system.

In the present study, we have developed a nHA-based nano-biomimetic gene carrier for plant transformation wherein the carrier does not remain in plant cells or disrupt cell function, and also less likelihood in horizontal transfer of heterologous genes to nontarget organisms. When combined with nuclease-based genome editing tools, the nHA-based approach does not result in the integration of gene editing components into the host genome as happens with other nanoparticle-mediated delivery approaches.[15,17] Indeed, our initial results suggest that this nano-biomimetic transformation system could allow stable transformation of crop species lines without multiple rounds of selection and breeding to remove the plasmid nanocarrier as required with carbon-based nanocarriers.[18] Hence, our nHA-based genetic transformation system could enable more rapid release of transformed plants from lab to field for analysis and various applications.[58] Our results indicate that the *in planta* nano-biomimetic plant transformation system we have developed is a sound nanoparticle-mediated approach that could be optimized for diverse biotechnological and agricultural applications in plant biology and crop science.

Conflicts of interest

There are no conflicts to declare.

Acknowledgements

The work was partially supported by South Dakota Board of Regents Competitive Research Grants #A18-0015-001 and #A20-0013-001 to B. W. M. W. This study was also partially funded by the University of South Dakota John W. Carlson Grant and Technology Readiness Acceleration Center (TRAC) Fellowship to C. L. I. We thank Mary Ann Cushman for technical editing assistance.

References

1 M. L. Zaidem, S. C. Groen and M. D. Purugganan, *Plant J.*, 2019, **97**, 40–55.
2 F. Altpeter, N. M. Springer, L. E. Bartley, A. E. Blechl, T. P. Brutnell, V. Citovsky, L. J. Conrad, S. B. Gelvin, D. P. Jackson, A. P. Kausch, P. G. Lemaux, J. I. Medford, M. L. Orozco-Cárdenas, D. M. Tricoli, J. Van Eck, D. F. Voytas, V. Walbot, K. Wang, Z. J. Zhang and C. N. Stewart, *Plant Cell*, 2016, **28**, 1510–1520.
3 J. K. Ma, P. M. Drake and P. Christou, *Nat. Rev. Genet.*, 2003, **4**, 794–805.
4 H. C. J. Godfray, J. R. Beddington, I. R. Crute, L. Haddad, D. Lawrence, J. F. Muir, J. Pretty, S. Robinson, S. M. Thomas and C. J. Toulmin, *Science*, 2010, **327**, 812–818.
5 A. Pereira, *Front. Plant Sci.*, 2016, **7**, 1123.
6 F. J. Cunningham, N. S. Goh, G. S. Demirer, J. L. Matos and M. P. Landry, *Trends Biotechnol.*, 2018, **36**, 882–897.
7 H. H. Hwang, M. Yu and E. M. Lai, *The Arabidopsis Book*, 2017, **15**, e0186.
8 L. G. Lowder, D. Zhang, N. J. Baltes, J. W. Paul, X. Tang, X. Zheng, D. F. Voytas, T.-F. Hsieh, Y. Zhang and Y. Qi, *Plant Physiol.*, 2015, **169**, 971–985.
9 R. Banakar, A. L. Eggenberger, K. Lee, D. A. Wright, K. Murugan, S. Zarecor, C. J. Lawrence-Dill, D. G. Sashital and K. Wang, *Sci. Rep.*, 2019, **9**, 19902.
10 S. B. Gelvin, *Microbiol. Mol. Biol. Rev.*, 2003, **67**, 16–37.
11 Y. Gleba, V. Klimyuk and S. Marillonnet, *Curr. Opin. Biotechnol.*, 2007, **18**, 134–141.
12 A. H. A. Rashid and D. D. Lateef, *Am. J. Plant Sci.*, 2016, **7**, 181–193.
13 F. Schwab, G. Zhai, M. Kern, A. Turner, J. L. Schnoor and M. R. Wiesner, *Nanotoxicology*, 2016, **10**, 257–278.
14 P. Wang, E. Lombi, F. J. Zhao and P. M. Kopittke, *Trends Plant Sci.*, 2016, **21**, 699–712.
15 G. S. Demirer, H. Zhang, J. L. Matos, N. S. Goh, F. J. Cunningham, Y. Sung, R. Chang, A. J. Aditham, L. Chio, M.-J. Cho, B. Staskawicz and M. P. Landry, *Nat. Nanotechnol.*, 2019, **14**, 456–464.
16 K. Deshmukh, S. R. Ramanan and M. Kowshik, *Mater. Sci. Eng., C*, 2019, **96**, 58–65.
17 P. Wang, F. J. Zhao and P. M. J. Kopittke, *Trends Plant Sci.*, 2019, **24**, 574–577.
18 S. Y. Kwak, T. T. S. Lew, C. J. Sweeney, V. B. Koman, M. H. Wong, K. Bohmert-Tatarev, K. D. Snell, J. S. Seo, N. H. Chua and M. Strano, *Nat. Nanotechnol.*, 2019, **14**, 447–455.
19 G. Chichiriccò and A. Poma, *Nanomaterials*, 2015, **5**, 851–873.
20 E. Kabir, V. Kumar, K. H. Kim, A. C. K. Yip and J. R. Sohn, *J. Environ. Manage.*, 2018, **225**, 261–271.
21 A. Montes, M. A. Bisson, J. A. Gardella and D. S. Aga, *Sci. Total Environ.*, 2017, **607–608**, 1497–1516.
22 S. K. Verma, A. K. Das, S. Gantait, V. Kumar and E. Gurel, *Sci. Total Environ.*, 2019, **667**, 485–499.
23 X. Yuan, X. Zhang, L. Sun, Y. Wei and X. Wei, *Part. Fibre Toxicol.*, 2019, **16**, 18.
24 M. Emamalipour, K. Seidi, S. Zununi Vahed, A. Jahanban-Esfahlan, M. Jaymand, H. Majdi, Z. Amoozgar, L. T. Chitkushev, T. Javaheri, R. Jahanban-Esfahlan and P. Zare, *Front. Cell Dev. Biol.*, 2020, **8**, 229.
25 S. Naqvi, A. N. Maitra, M. Z. Abdin, M. Akmal, I. Arora and M. Samim, *J. Mater. Chem.*, 2012, **22**, 3500–3507.
26 M. S. O. Rafsanjani, U. Kiran, A. Ali and M. Abdin, *Indian J. Biotechnol.*, 2016, **2**, 145–152.
27 Y. Cai, Y. Liu, W. Yan, Q. Hu, J. Tao, M. Zhang, Z. Shi and R. Tang, *J. Mater. Chem.*, 2007, **17**, 3780–3787.
28 S. H. Zhu, B. Y. Huang, K. C. Zhou, S. P. Huang, F. Liu, Y. M. Li, Z. G. Xue and Z. G. Long, *J. Nanopart. Res.*, 2004, **6**, 307–311.
29 T. N. Tram Do, W. H. Lee, C. Y. Loo, A. V. Zavgorodniy and R. J. T. D. Rohanizadeh, *Ther. Delivery*, 2012, **3**, 623–632.
30 F. Bakan, *Hydroxyapatite*, 2018, **14**, 157–176.
31 L. J. del Valle, O. Bertran, G. Chaves, G. Revilla-López, M. Rivas, M. T. Casas, J. Casanovas, P. Turon, J. Puiggalí and C. Alemán, *J. Mater. Chem. B*, 2014, **2**, 6953–6966.
32 K. Deshmukh, S. R. Ramanan and M. Kowshik, *Nanoscale Adv.*, 2019, **1**, 3015–3022.
33 P. Turon, L. J. Del Valle, C. Alemán and J. Puiggalí, *Appl. Sci.*, 2017, **7**, 60.
34 A. Priyam, R. K. Das, A. Schultz and P. P. Singh, *Sci. Rep.*, 2019, **9**, 15083.
35 M. B. Taşkın, Ö. Şahin, H. Taskin, O. Atakol, A. Inal and A. Gunes, *J. Plant Nutr.*, 2018, **41**, 1148–1154.
36 R. Nair, S. H. Varghese, B. G. Nair, T. Maekawa, Y. Yoshida and D. S. Kumar, *Plant Sci.*, 2010, **179**, 154–163.
37 A. Singh, N. Singh, I. Hussain, H. Singh and S. Singh, *Int. J. Pharm. Sci.*, 2015, **4**, 2319–6718.
38 N. Bala, A. Dey, S. Das, R. Basu and P. Nandy, *Iran. J. Plant Physiol.*, 2014, **4**, 1061–1069.
39 L. Marchiol, A. Filippi, A. Adamiano, L. Degli Esposti, M. Iafisco, A. Mattiello, E. Petrussa and E. Braidot, *Agronomy*, 2019, **9**, 161.
40 J. Hwang, Y. Jeong, J. M. Park, K. H. Lee, J. W. Hong and J. Choi, *Int. J. Nanomed.*, 2015, **10**, 5701–5713.
41 A. Li, J. Zhao, J. Fu, J. Cai and P. Zhang, *Asian J. Pharm. Sci.*, 2019, **21**, 41.
42 N. Suresh Kumar, R. Padma Suvarna, K. Chandra Babu Naidu, P. Banerjee, A. Ratnamala and H. H. Manjunatha, *Appl. Phys. A: Mater. Sci. Process.*, 2020, **126**, 1–8.
43 F. Huang, Y. Shen, A. Xie, J. Zhu, C. Zhang, S. Li and J. J. J. Zhu, *J. Mater. Sci.*, 2007, **42**, 8599–8605.
44 N. A. Alcantar, E. S. Aydil and J. N. Israelachvili, *J. Biomed. Mater. Res.*, 2000, **51**, 343–351.
45 R. Liu and R. Lal, *Sci. Rep.*, 2014, **4**, 5686.
46 A. A. Wise, Z. Liu and A. N. Binns, *Agrobacterium Protocols*, ed. K. Wang, Humana Press, USA, 2nd edn, 2006, vol. 3, pp. 43–54.
47 K. Leuzinger, M. Dent, J. Hurtado, J. Stahnke, H. Lai, X. Zhou and Q. J. J. Chen, *J. Visualized Exp.*, 2013, **77**, 50521.
48 S. D. Lim, W. C. Yim, D. Liu, R. Hu, X. Yang and J. C. Cushman, *Plant Biotechnol. J.*, 2018, **16**, 1595–1615.

49 P. C. Ray, H. Yu and P. P. Fu, *J. Environ. Sci. Health, Part C: Environ. Carcinog. Ecotoxicol. Rev.*, 2009, **27**, 1–35.
50 S. Kumar, A. K. Patra, S. C. Datta, K. G. Rosin and T. J. Purakayastha, Phytotoxicity of nanoparticles to seed germination of plants, *Int. J. Curr. Adv. Res.*, 2015, **3**, 854–865.
51 D. K. Tripathi, S. Singh, S. Singh, R. Pandey, V. P. Singh, N. C. Sharma, S. M. Prasad, N. K. Dubey and D. K. Chauhan, *Plant Physiol. Biochem.*, 2017, **110**, 2–12.
52 M. Yang and M. Zhang, *Front. Mater.*, 2019, **6**, 225.
53 Z. Javed, K. Dashora, M. Mishra, V. D. Fasake and A. Srivastva, *Nanosci. Nanotechnol.*, 2019, **5**, 1–9.
54 W. Broothaerts, H. J. Mitchell, B. Weir, S. Kaines, L. M. Smith, W. Yang, J. E. Mayer, C. Roa-Rodriguez and R. A. J. N. Jefferson, *Nature*, 2005, **433**, 629–633.
55 L. T. Dunning, J. K. Olofsson, C. Parisod, R. R. Choudhury, J. J. Moreno-Villena, Y. Yang, J. Dionora, W. P. Quick, M. Park, J. L. Bennetzen, G. Besnard, P. Nosil, C. P. Osborne and P. A. Christin, *Proc. Natl. Acad. Sci. U. S. A.*, 2019, **116**, 4416–4425.
56 Z. Qiu, Y. Yu, Z. Chen, M. Jin, D. Yang, Z. Zhao, J. Wang, Z. Shen, X. Wang, D. Qian, A. Huang, B. Zhang and J.-W. Li, *Proc. Natl. Acad. Sci. U. S. A.*, 2012, **109**, 4944–4949.
57 X. X. Ye, G. Z. Wang, Y. X. Zhang and H. J. Zhao, *Environ. Sci.: Nano*, 2018, **5**, 398–407.
58 A. Pérez-de-Luque, *Front. Environ. Sci.*, 2017, **5**, 12.